Prediction of Laminar-Turbulent Transition on an Airfoil at High Level of Free-Stream Turbulence

Valery Chernoray
Department of Applied Mechanics, Chalmers University of Technology
412 96 Göteborg, Sweden

Abstract
Prediction of laminar-turbulent transition at high level of free-stream turbulence in boundary layers of airfoil geometries with external pressure gradient changeover is in focus. The aim is a validation of a transition model for transition prediction in turbomachinery applications. Numerical simulations have been performed by using a transition model by Langtry and Menter for a number of different cases of pressure gradient, at Reynolds number-range, based on the airfoil chord, $50\,000 \leq Re \leq 500\,000$ and free-stream turbulence intensities 2 % and 4 %. The validation of the computational results against the experimental data showed good performance of used turbulence model for all test cases.

1. Introduction

Components of an aero-engine operate in a Reynolds number range between $5\cdot10^4$ and $1\cdot10^6$ [1]. For this range of Reynolds numbers, the laminar-turbulent transition in a boundary layer and separation are playing an important role in determining the flow and heat transfer. In order to predict the aerodynamic and heat transfer performance of aero-engine components accurately one need to predict the location and length of the regions with laminar-turbulent transition and separation. This prediction is a challenging task due to the presence of varying pressure gradients and high level of free-stream turbulence.

Except for the fan, the level of turbulence in an aero-engine is high, above 1 %, and classic transition scenario is seldom realized. The typical transition regimes are the bypass transition and separated flow transition. An overview of different scenario of laminar-turbulent transition at high free-stream turbulence and pressure gradient can be found in studies [2-6]. On an airfoil, if the Reynolds number is high enough so that the transition is complete before a laminar separation can occur or if the boundary layer does not separate because the flow deceleration is slight, then an attached flow transition occurs. If the adverse pressure gradient is more severe and the Reynolds number is low, then the laminar boundary layer tends to separate and transition occurs in the free shear layer of the separation bubble. This scenario is called a separated flow transition. This type of transition typically may occur near an airfoil leading edge on suction or pressure side, or both, and near the point of minimum pressure on the suction side. At intermediate Reynolds numbers, the transition occurs in the attached flow ahead of the location where the laminar boundary layer would separate.

If the component must operate over a wide range of Reynolds numbers and angles of incidence all above scenarios can occur at different flow regimes. Such situations are particularly difficult for turbulence modelling.

A number of turbulence models claim a possibility of transition prediction but none of them is proven to be flawless so far. A transition model suggested by Menter et al. [7] is based on correlation-based approach which appears to provide consistent results. This model has been applied to a number of 2D and 3D test flow cases [8] and simulations agreed well with experiments for studied cases at wide range of Reynolds numbers and freestream turbulent intensities. However, a literature survey shows that not so many other validation cases of this model are publicly available. To fulfil this gap and to validate the applicability of model by Langtry and Menter for cases with different pressure gradient, turbulence intensity and Reynolds number is the main purpose of current study.

2. Experimental and numerical setup

2.1 Airfoil models

The experiments were specially designed for validation of boundary layer transition and for detailed measurement of the boundary layer development on an airfoil. In order to provide the measurements of boundary layers with good spatial resolution large-scale airfoil test models were used. Several different airfoil geometries were selected to model the effect of different pressure gradient distributions. Since the range of flow Reynolds numbers of interest for current study is $5 \cdot 10^4$—$5 \cdot 10^5$ (based on the chord) and the incoming flow turbulence intensity is above 2 %, the aft part of the airfoil was not of interest. Thus truncated airfoil models with the aft part replaced by a straight section, see Fig. 1, were designed and manufactured. This design is advantageous due to a simpler manufacturing and makes the near wall-measurements easier.

Fig. 1 shows a modified model with straight aft part and a full airfoil superimposed on corresponding pressure distributions. One can observe that for the modified model the magnitude of the pressure peak is decreased by 25 % and the magnitude of the favourable pressure gradient in the accelerated region is decreased correspondingly, while the adverse pressure gradient become stronger directly after the pressure minimum with a zone of a milder gradient further downstream. Apart from these differences the pressure distribution for the modified model is a typical airfoil-like pressure distribution with characteristic pressure gradient changeover.

To cover a range of pressure gradient distributions typical for turbomachinery applications four different airfoil nose shapes were developed. The geometry of the models and corresponding pressure distributions obtained numerically are shown in Fig. 2. The model shapes were designed based on NACA6 airfoil of two different modifications and with two different aspect ratios. Case 1 and Case 2 are thickened versions of Case 3 and Case 4 by a factor of two. Correspondingly, the pressure minimum for these models is twice larger in magnitude compared to Case 3 and Case 4 (the values are –1.2 and –0.6 correspondingly). Case 1 and Case 3 both have the location of pressure minimum shifted towards the leading edge which results in a stronger favourable pressure gradient and slightly milder adverse pressure gradient compared to Cases 2 and 4. Overall, the favourable pressure gradient is the strongest for Case 1 and gradually decreasing for Cases 2, 3 and 4.

Current Cases 1 and 2 are modelling the pressure distribution of high- and medium-loaded turbomachinery vanes (cf. [9]) and Cases 3 and 4 have typical pressure distributions for low-loaded vanes [10].

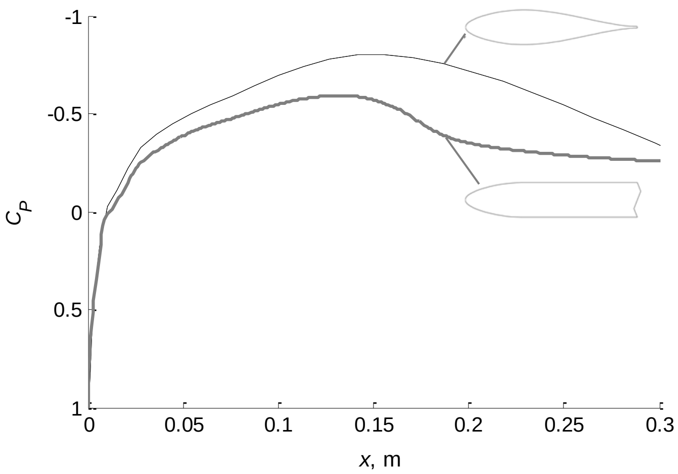

Figure 1: Comparison of pressure distributions on a full airfoil and on airfoil model with straight aft part. The straight section starts at x = 0.16 m.

2.2 Experimental setup

Experiments were performed in a wind tunnel facility at Chalmers. Used tunnel is of open circuit type and was operated at velocities between 5 and 18 m/s. The cross section of the facility is 200 by 1200 mm. Since the thickness of the airfoil models was 100 mm the blockage of the wind-tunnel was 8 %. Note, however, that all presented CFD results were obtained with the blockage effect taken into account since calculations were performed for same size of the numerical wind-tunnel as in experiments, thus the blockage has no influence on the discussed results.

In the wind-tunnel the test section is equipped with an end-wall boundary-layer suction system for removal of sidewall boundary layers, which allowed obtaining the flow with good two-dimensionality.

The airfoil test models are manufactured by using a stereo lithography technique which has a typical accuracy of ± 0.1 % of the model size. Models produced by this method have small traces on the surface due to a finite resolution of the SLA machine. For obtaining smooth surfaces an epoxy coating was applied on the models and thereafter the surfaces were polished.

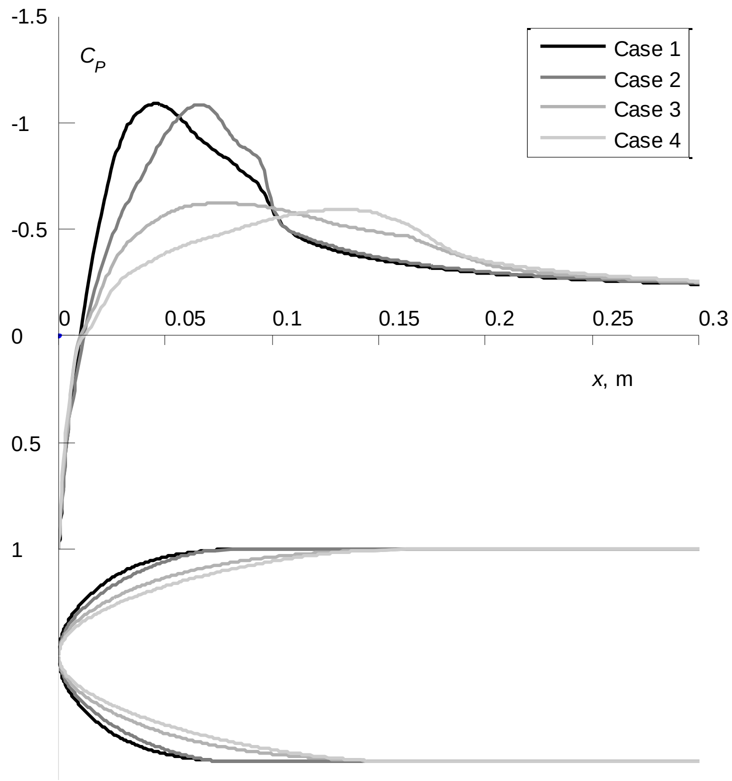

Figure 2: Pressure distributions for four studied airfoil models

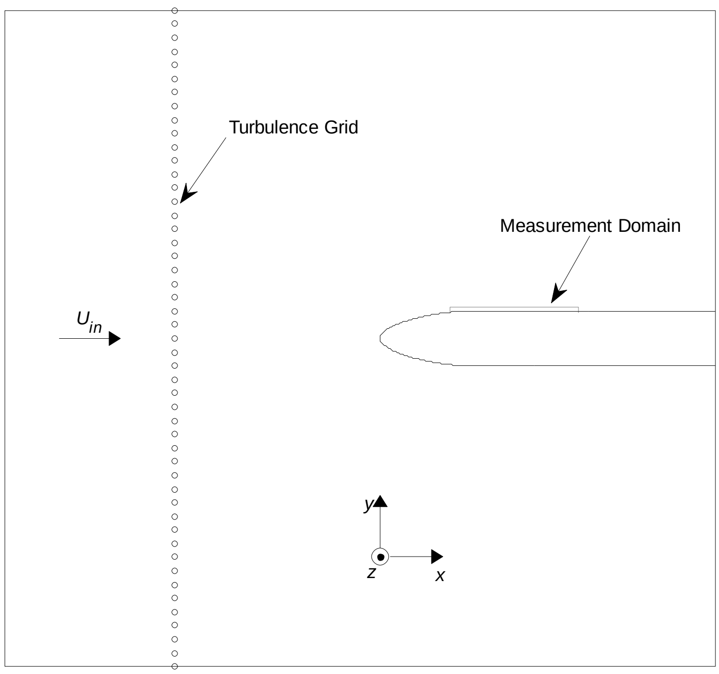

Figure 3: Experimental setup

For monitoring of the static pressure distributions each model was equipped with 15 pressure taps distributed along the streamwise direction.

A turbulence grid is used to create an elevated turbulence intensity of the inflow. The grid is built of 5 mm bars of circular cross-section and a mesh size of the grid, *M*, is 25 mm, thus giving a porosity (ratio between open and total area of the grid) of 0.64. A 1-mm thick wire was additionally spirally coiled around the grid bars in order to decrease the mean-velocity modulation in the wakes behind the bars. The grid was placed at 800 mm upstream of an airfoil model ($x / M = 32$) in configuration of 2 % incoming flow turbulence intensity and at 270 mm upstream of a model ($x / M = 11$) in case of 4 % turbulence intensity. The turbulence intensity was measured at the model leading edge. The turbulence length scale and turbulence anisotropy generated by this grid were evaluated earlier [9] by using cross-hot-wire measurements. It is of importance to note that in current CFD simulations the turbulence intensity and turbulence length scale were adjusted at the inlet of CFD domain to match the both respective values in CFD and experiment at the airfoil leading edge.

The boundary layer measurements were performed by using a constant temperature hot-wire anemometer. A single-wire probe was used with a tungsten wire of 3 mm length and 5 μm in diameter. The probe calibration was performed in a dedicated calibrator. The maximum error in the probe calibration was within 0.5 % for all calibration points. Probe positioning and data acquisition were fully automated. A three-axis probe positioning system has resolution of 1.6 μm. The boundary layer profiles were measured at the mid-span at 16 streamwise locations with 27 points in each profile. The measurements were repeated for each of 18 investigated flow cases.

The inlet flow velocity in the wind-tunnel was monitored by a Pitot-Prandtl tube connected to a digital micro-manometer, which had sensors for temperature and absolute pressure readings. Surface static pressure distributions were measured by a 16-channel PSI 9116 digital pressure scanner (Pressure System Inc.) which has a measuring range of ±2500 Pa. The accuracy of the scanner in the measurement range of current experiment (±250 Pa) is ±2 Pa. The measured surface pressure distributions agreed well with the numerical distributions shown in Fig. 2. The curve shape and the location of pressure minimum were captured well by CFD and the magnitude of the pressure minimum has agreed within 10 % between CFD and experiments. These results can be found in work [11].

2.3 Numerical setup

Numerical calculations were performed with Gamma-Theta transition turbulence model by Langtry and Menter [6]. This correlation-based model uses transport equations for intermittency and momentum thickness Reynolds number. The intermittency equation is coupled with Menter's $k — \omega$ SST model and used to turn on the production of the turbulent kinetic energy beyond the turbulent transition region. The second transport equation is formulated in terms of the momentum thickness Reynolds number at the transition onset. An empirical correlation is used to control the transition onset criteria in the intermittency equation.

In current study steady two-dimensional computations were performed by using pressure based implicit finite volume solver and second-order discretization of equations. The computational grid consists of an O-grid surrounding the model, which is shown in Fig. 4 by black colour. The grid in the free-stream consists of a block with quadrilateral cells (light-grey region in Fig. 4) and a block with unstructured grid (shown by dark-grey colour).

The baseline grid has 10^5 cells with the first row of cells at $y^+ < 0.5$. For the grid independency check two additional grids, a refined and coarsened, were used. The refined grid uses $7 \cdot 10^5$ cells (with $y^+ < 0.25$) and the coarsened grid has same number of cells as the baseline grid with only the O-grid part coarsened, but in such a way that the grid y^+ values are below 1. The calculations on three different grids were performed for 6 of presented flow cases.

The boundary conditions in numerical calculations are carefully matched with corresponding conditions from the wind tunnel tests. The turbulence intensity and turbulent length scale at the inlet are adjusted so that at the airfoil leading edge the values were equal in CFD and experiments.

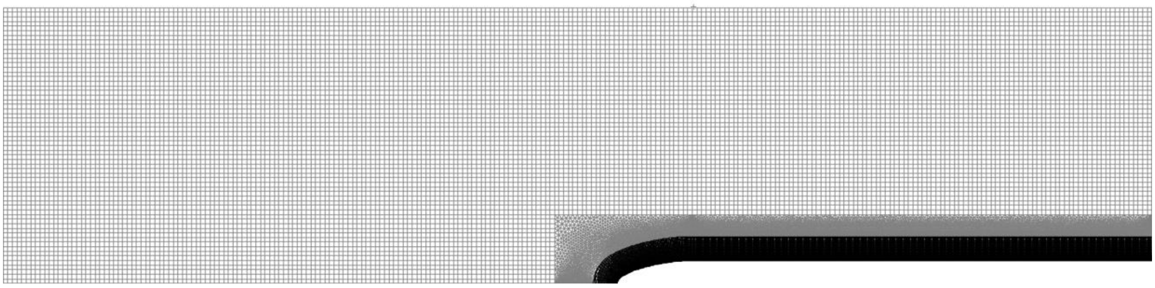

Figure 4: Computational grid

3. Results

In this paper the results are presented from 9 test cases of total 18, the rest of experimental and numerical data can be found in report [11].

In Fig. 5 a set of profiles of mean velocity and turbulence intensity are shown for Case 4 at inlet velocity 9 m/s and free stream turbulence intensity 2 %. Case 4 is a case of mild pressure gradient and the velocity 9 m/s represents the medium of three studied velocities 5, 9 and 18 m/s. Note that the profiles are for every third of all measured *x*-stations.

From the mean velocity profiles it is clearly seen that in this case, the boundary layer is initially laminar and the initial profile at x = 0.13 m has shape close to the Blasius velocity profile, which is depicted for comparison. For the next measurement point at x = 0.22 m the action of adverse pressure gradient results in a less full profile than the Blasius profile. The profile of the turbulence intensity at the first measurement station has a typical distribution for a laminar boundary layer subjected to high turbulence intensity. One can observe that the magnitude of turbulence increases from the free-stream value of 2 % to 8 % inside the boundary layer. This peak value is located in the middle of the boundary layer at $y = 3.5\theta$. At next streamwise position, x = 0.22 m, the laminar-turbulent transition starts and proceeds until x = 0.28 m. The maximum turbulence intensity near the wall is 14 % in the middle of the transitional range at x = 0.25 m. As seen, from x = 0.25 m the position of the maximum r.m.s. in the boundary layer is shifted towards the wall, and at x = 0.28 m the shape of the r.m.s. profile become typical for a turbulent boundary layer. The last two measurement stations, x = 0.31 and x = 0.34 m reveal typical distributions of the mean velocity and turbulence intensity for a turbulent boundary layer with observable similarity for both the mean and r.m.s. velocity profiles.

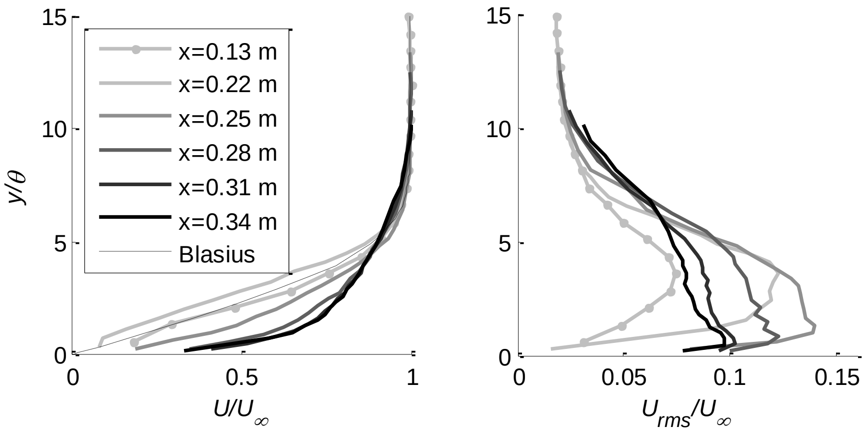

Figure 5: Boundary layer profiles of mean velocity and turbulence intensity for Case 4 at inlet velocity U_{in}=9 m/s and inlet turbulence intensity Tu_{in}=2 %. Dashed line shows Blasius velocity profile.

3.2 Effect of Reynolds Number

Figure 6 shows contour plots of turbulence intensity within the boundary layer for Case 4 at different inflow Reynolds numbers. It is seen that the turbulent region in the boundary layer moves upstream as flow Reynolds number increases. The intermittency contours are helping to highlight the transition start and end. Transition location is where the intermittency is 0.5. The lowest inlet flow Reynolds number produces the longest transitional region as expected.

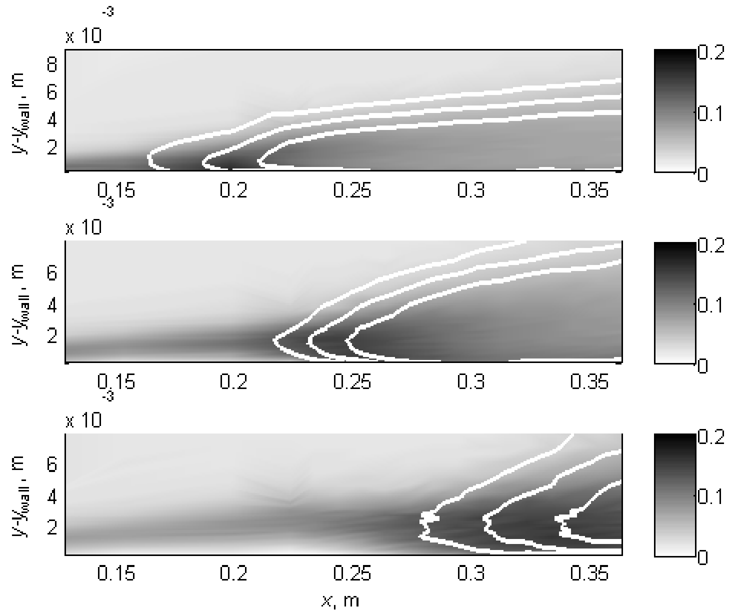

Figure 6: Effect of inlet Reynolds number on boundary layer transition for case of mild pressure gradient (Case 4) at Tu_{in} = 2 %. Inlet velocity U_{in} = 5, 9 and 18 m/s (from bottom to top). Pseudo-colours depict local turbulence intensity U_{rms} / U_{in} and white contour lines depict intermittency levels of 0.25, 0.5 and 0.75.

3.3 Effect of Pressure Gradient

Contour plots in Figure 7 show turbulence intensity distributions for two cases of different pressure gradient. The top plot of figure shows measurements for the case of stronger pressure gradient in Case 2 and the bottom plot is for Case 4. One can observe that the transition point moves upstream when a stronger adverse pressure gradient is present. At the same speed and free-stream turbulence level, the effect of increasing the adverse pressure gradient is, as might be expected, an earlier transition beginning.

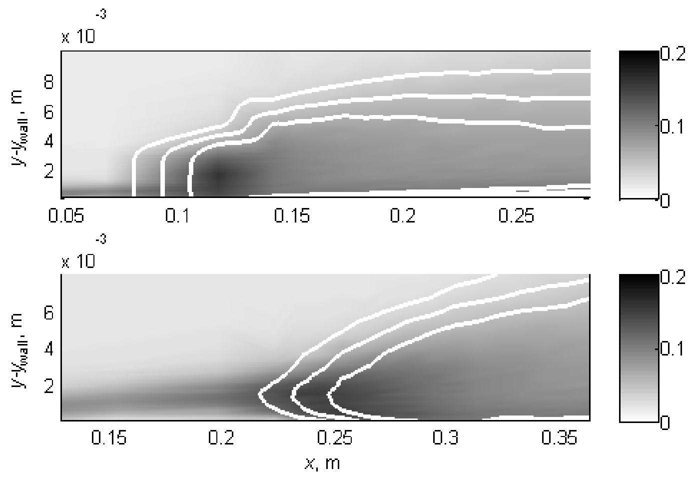

Figure 7: Effect of pressure gradient. Top figure shows case of strong pressure gradient (Case 2) and bottom shows case of mild pressure gradient (Case 4) at U_{in} = 9 m/s, Tu_{in} = 2 %. Note different streamwise axes. Pseudo-colours depict local turbulence intensity U_{rms} / U_{in} and white contour lines depict intermittency levels of 0.25, 0.5 and 0.75.

3.4 Effect of Inlet Turbulence Intensity

The contour plot in Figure 8 shows the effect of varying free-stream turbulence. The case of elevated turbulence intensity, Tu = 4 %, is shown in comparison with previously discussed case of Tu = 2 %. As expected, higher level of freestream turbulence promotes the transition onset. It is noticeable that in case of Tu = 4 % the transition begins already in the zone of favourable pressure gradient.

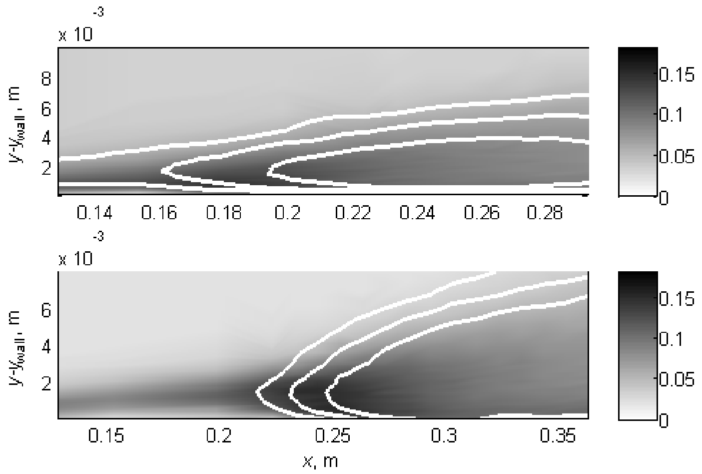

Figure 8: Effect of inlet turbulence intensity. Top figure shows case of Tu_{in} = 4 % and bottom Tu_{in} = 2 % for Case 4 at U_{in} = 9 m/s. Pseudo-colours depict local turbulence intensity U_{rms} / U_{in} and white contour lines depict intermittency levels of 0.25, 0.5 and 0.75.

3.5 Validation of CFD results

In this section the results of CFD calculations are presented. The calculations are validated by the experimental data. For validation we selected to compare distributions of the momentum thickness Reynolds number and distributions of the shape factor, H_{12}.

Figure 9 shows the results of comparison between CFD and experiment for case of mild pressure gradient (Case 4) at turbulence intensity, Tu_{in} = 2 %. Results are shown for inlet velocities, U_{in} = 5, 9 and 18 m/s. The CFD results are shown from calculations on 3 different grids to demonstrate the grid independency. The development of the momentum thickness Reynolds number is captured very well by CFD in all cases of inlet velocity. The shape factor distributions are predicted the best for the highest inlet velocity, 18 m/s. At two cases of lower inlet velocity the transition occurs earlier in CFD. For case of 9 m/s inlet velocity the transition in CFD starts already at the beginning of the shown interval, at x = 0.15 m, while in experiment the transition begins at x = 0.2 m. The transition location is over-predicted by 0.05 m, which would correspond to 10 % of the cord assuming the equivalent chord of 0.5 m. In experiment the transition occurs at the end of the zone with adverse pressure gradient and in CFD at the beginning of this zone, just downstream of the pressure minimum. For case of 5 m/s the transition in CFD starts at x = 0.2 m, while in experiment the transition begins at x = 0.27 m. The transition location over-prediction is 0.07 m. In both CFD and experiment the transition occurs at the end of the zone with adverse pressure gradient.

One can note that the experimental values of the shape factor agree with the pressure distributions and demonstrate reasonable behaviour. Particularly at the pressure minimum the shape factor is close to the shape factor for the Blasius boundary layer which is 2.59. Through the measurement region the shape factor is below the value for the laminar separation which is 3.85 and at the end of the measured region for the highest Reynolds number case the shape factor is approaching the value for the developed turbulent boundary layer on a flat plate, which is 1.3.

Experimental transition locations in terms of Re_θ are correspondingly 200, 250 and 300 for velocities 5, 9 and 18 m/s. In CFD the transition occurs for Re_θ = 200 in all cases. The results of current experiments agree well with earlier reported values 250-300 [1, 6] for 2 % turbulence intensity.

In case of stronger pressure gradient the results are shown in Fig. 10. The agreement of CFD and experiment is very good for Re_θ and H_{12} distributions. The transition occurs at x = 0.07 m both in CFD and experiment. This is the location just behind the pressure minimum. The transition Reynolds number from experiments is 100, 150 and 200 for velocities 5, 9 and 18 m/s.

For the cases when the turbulence intensity was increased to 4 % the results are presented in Fig. 11. In this case the CFD results are shown from 3 different grids to demonstrate the grid independency. The development of the momentum thickness Reynolds number is captured very well by CFD in all cases. The shape factor distributions are predicted the best for the medium inlet velocity, 9 m/s. For the case of lower inlet velocity, 5 m/s the transition occurs earlier in CFD by about 0.03 m, which would correspond to 6 % of chord at equivalent chord of 0.5 m. For case of 18 m/s the transition location is under-predicted by about 0.05 m. The experimental data do not extend far enough upstream to make a more precise conclusion. Both in CFD and experiment the transition starts in the zone of favourable pressure gradient at 18 m/s. The transition Reynolds number in experiment is around 200 in all three cases which agrees well with reported in [1, 6] interval 150-200.

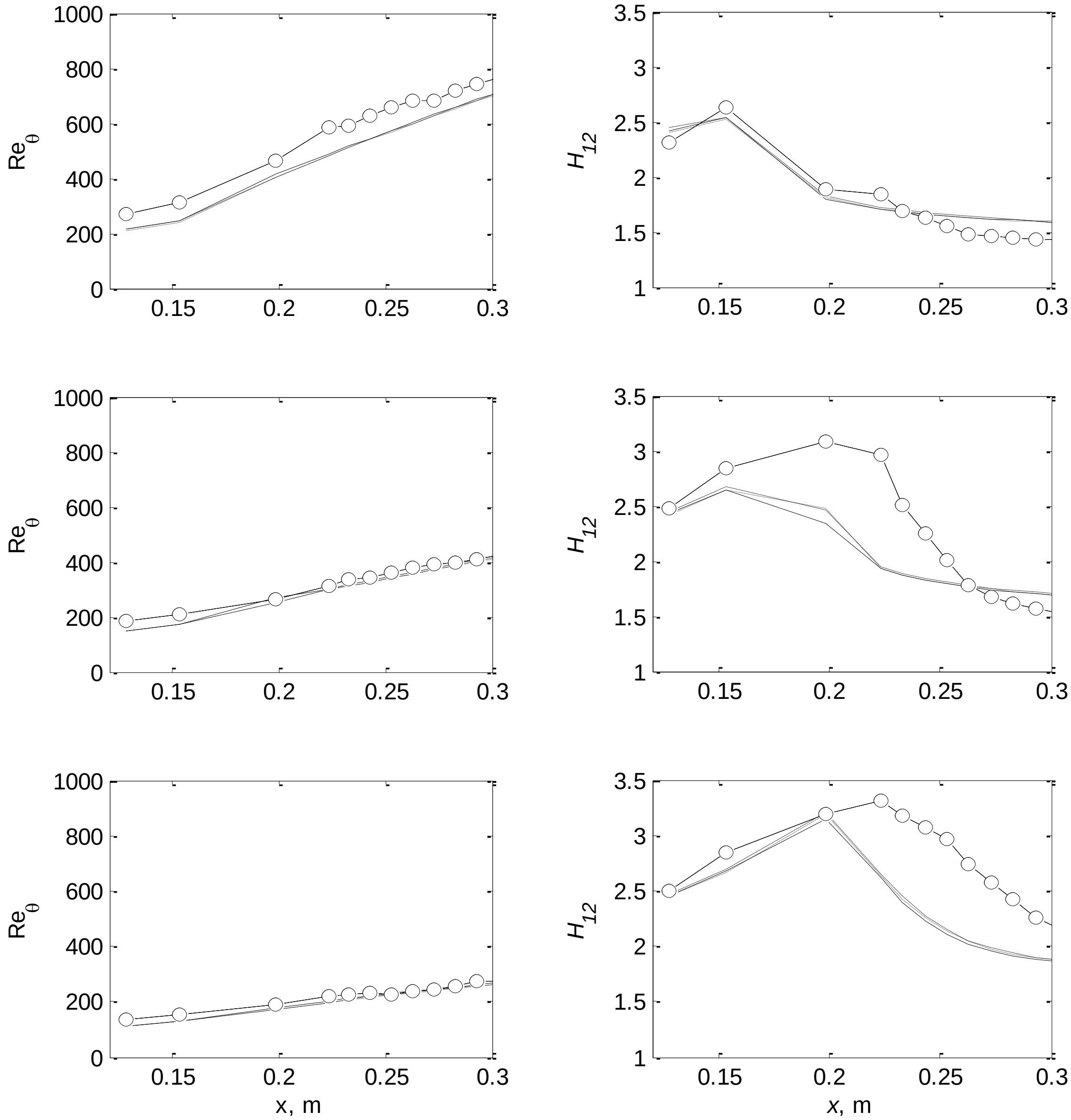

Figure 9: Comparison of experiment and CFD at Tu_{in} = 2 % for case of mild pressure gradient (Case 4) and U_{in} = 5, 9 and 18 m/s (from bottom to top). Symbols show experimental data and lines are CFD results on 3 different meshes.

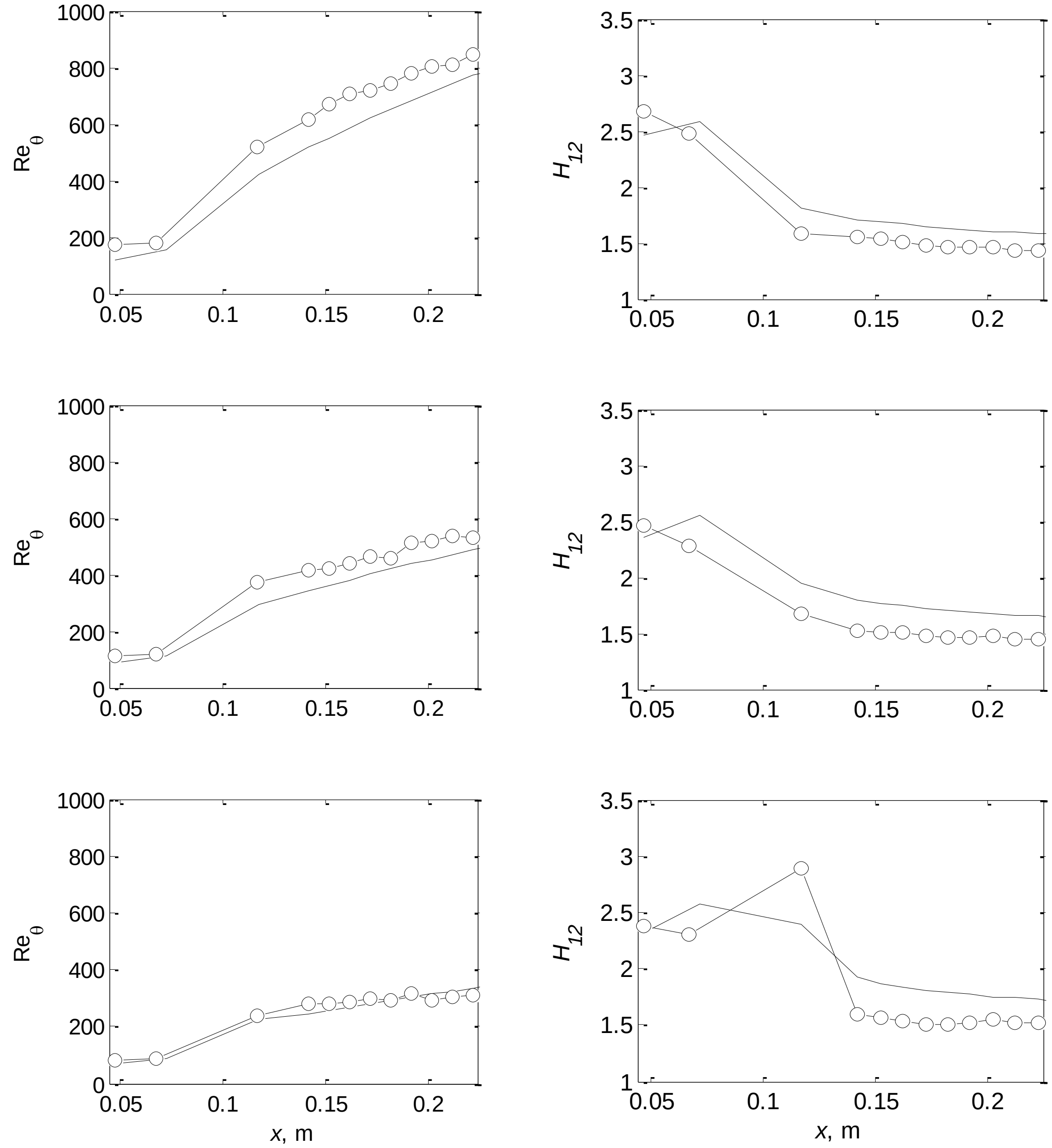

Figure 10: Comparison of experiment and CFD at Tu_{in} = 2 % for case of strong pressure gradient (Case 2) and U_{in} = 5, 9 and 18 m/s (from bottom to top). Symbols show experimental data and lines are CFD results from a medium-size grid calculations.

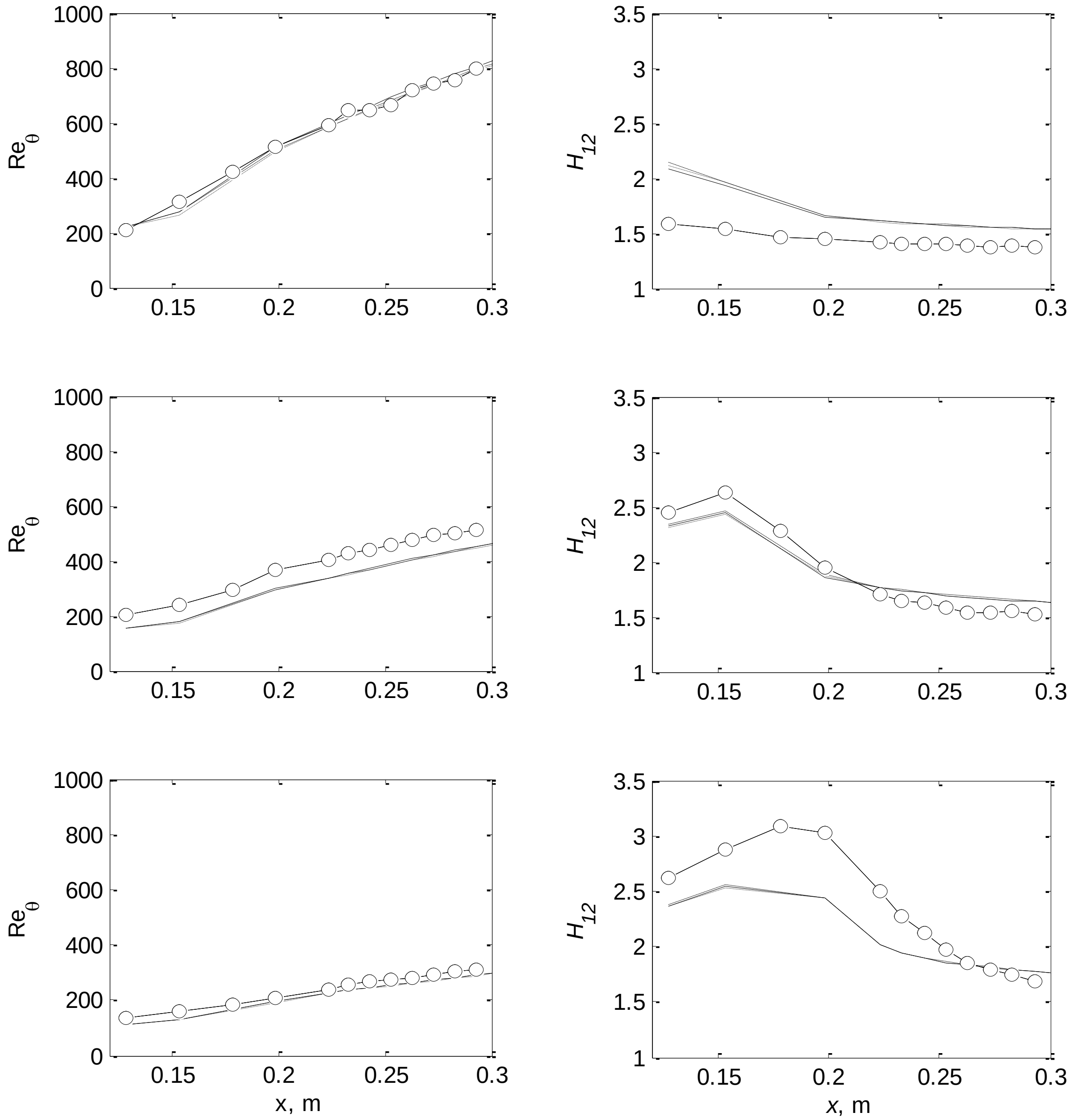

Figure 11: Comparison of experiment and CFD at Tu_{in} = 4 % for case of mild pressure gradient (Case 4) and U_{in} = 5, 9 and 18 m/s (from bottom to top). Symbols show experimental data and lines are CFD results on 3 different meshes.

Conclusions

Laminar-turbulent transition at high free-stream turbulence in boundary layers of the airfoil-like geometries with presence of the external pressure gradient changeover has been studied numerically and validated by experimental data. The comparison is performed for a number of flow cases with different flow Reynolds number, turbulence intensity and pressure distributions. The flow parameters selected are typical for turbomachinery applications.

The numerical calculations by using SST model with transition by Langtry and Menter show encouraging results. CFD shows very good prediction of transition location for cases with strong pressure gradient for turbulence levels 2 % and 4 %. In case of mild pressure gradient CFD computations demonstrate reasonably good predictions with some under- or over-prediction of the transition onset.

References

[1] Mayle R. E. 1991. The 1991 IGTI Scholar Lecture: The role of laminar-turbulent transition in gas turbine engines, *ASME J. of Turbomach.* 113, pp. 509-537.

[2] Abu-Ghannam B. J., Shaw R. 1980. Natural transition of boundary layers-the effects of turbulence, pressure gradient, and flow history, *IMechE J.l Mech. Eng. Sci.* 22, pp. 213-228.

[3] Walker G. J., Gostelow J. P. 1990. Effects of adverse pressure gradients on the nature and length of boundary-layer transition, *ASME J. of Turbomach.*, 112, pp. 196-205.

[4] Gostelow J. P., Blunden A. R. and Walker G. J. 1994. Effects of freestream turbulence and adverse pressure gradients on boundary-layer transition, *ASME J. of Turbomach.*, 116, pp. 392-404.

[5] Solomon W. J., Walker G. J. and Gostelow J. P. 1996. Transition length prediction for flows with rapidly changing pressure gradients, *ASME J. of Turbomach.*, 118, pp. 744-751.

[6] Blair, M. F. 1982. Influence of free-stream turbulence on boundary layer transition in favourable pressure gradients. *J. Engng. for Power*, Vol. 104, pp. 743-750.

[7] Menter, F. R., Langtry, R. B., Likki, S. R., Suzen, Y. B., Huang, P. G., and Völker, S. 2004. A correlation based transition model using local variables Part 1 – Model formulation, *ASME Paper* GT2004-53452.

[8] Langtry, R. B., Menter, F. R., Likki, S. R., Suzen, Y. B., Huang, P. G., and Völker, S. 2004. A correlation based transition model using local variables Part 2 – Test cases and industrial applications, *ASME Paper* GT2004-53454.

[9] Chernoray, V., Ore, S., Larsson, J. 2010. Effect of geometry deviations on the aerodynamic performance of an outlet guide vane cascade. In *Proc. of ASME Turbo Expo 2010*, Paper GT2010-22923.

[10] Johansson, M., Chernoray, V., Ström, L., Larsson, J., Abrahamsson, H., 2011. Experimental and numerical investigation of an aerodynamically loaded guide vane in a turbine duct. In *Proc. of ASME Turbo Expo 2011*, Paper no GT2011-46221.

[11] Niebles Atencio B. M. 2011. Measurements and prediction of laminar-turbulent transition at high free-stream turbulence in boundary layers with pressure gradients. *MSc Thesis*, Chalmers University of technology.

[12] Boiko, A. V., Dovgal, A. V., Grek, G. R., Kozlov, V. V. 2002. “The origin of turbulence in near-wall flows”, Springer-Verlag.